Jet stream dynamics, hydroclimate, and fire in California from 1600 CE to present

Eugene R. Wahl[a,1], Eduardo Zorita[b], Valerie Trouet[c], and Alan H. Taylor[d,e]

[a]Center for Weather and Climate, National Centers for Environmental Information, National Oceanic Atmospheric Administration, Boulder, CO 80301; [b]Institute of Coastal Research, Helmholz-Zentrum Geesthacht, 21502 Geesthacht, Germany; [c]Laboratory of Tree-Ring Research, University of Arizona, Tucson, AZ 85721; [d]Department of Geography, Pennsylvania State University, University Park, PA 16802; and [e]Earth and Environmental Systems Institute, Pennsylvania State University, University Park, PA 16802

Moisture delivery in California is largely regulated by the strength and position of the North Pacific jet stream (NPJ), winter high-altitude winds that influence regional hydroclimate and forest fire during the following warm season. We use climate model simulations and paleoclimate data to reconstruct winter NPJ characteristics back to 1571 CE to identify the influence of NPJ behavior on moisture and forest fire extremes in California before and during the more recent period of fire suppression. Maximum zonal NPJ velocity is lower and northward shifted and has a larger latitudinal spread during presuppression dry and high-fire extremes. Conversely, maximum zonal NPJ is higher and southward shifted, with narrower latitudinal spread during wet and low-fire extremes. These NPJ, precipitation, and fire associations hold across pre–20th-century socioecological fire regimes, including Native American burning, postcontact disruption and native population decline, and intensification of forest use during the later 19th century. Precipitation extremes and NPJ behavior remain linked in the 20th and 21st centuries, but fire extremes become uncoupled due to fire suppression after 1900. Simulated future conditions in California include more wet-season moisture as rain (and less as snow), a longer fire season, and higher temperatures, leading to drier fire-season conditions independent of 21st-century precipitation changes. Assuming continuation of current fire management practices, thermodynamic warming is expected to override the dynamical influence of the NPJ on climate–fire relationships controlling fire extremes in California. Recent widespread fires in California in association with wet extremes may be early evidence of this change.

jet stream | precipitation | fire | California | paleoclimatology

The severe drought experienced in California (CA) from 2012 to 2015 CE (CE is omitted hereafter) impacted its economy and environment, reducing water availability for urban and agriculture consumers as well as for hydroelectric power generation (1), and increasing tree mortality and wildfire risk (2). High precipitation events in the wet seasons of 2016 and 2017 relieved immediate effects of this four-year drought, but their magnitude highlights the problematic nature of precipitation extremes and the need to simultaneously cope with the effects of both severe drought and flooding (3). The extreme nature of the polarities—exemplified by a 500-y record-low Sierra Nevada snowpack in 2015 (4), followed by threats to major dam integrity and widespread flooding (5) along with the 676,000 ha burned to date (January 1 to December 2) in 2018 (6), which caused the greatest loss of life in CA history—raises questions about the contribution of anthropogenic climate change to these events and its future impacts. Extreme drought in CA occurs when low winter precipitation coincides with unusually high temperatures, and these conditions have become more frequent with rising temperatures in recent decades (7). In extreme warm/wet years such as 2017, with very deep Sierra Nevada snowpack and abundant precipitation, intense rainfall can result in large floods and power outages (8). High spring and summer temperatures rapidly desiccate the abundant fuels produced by the high precipitation and, when combined with high winds, can greatly increase area burned and loss of life in wildfires that are difficult to control, as exemplified by the Tubbs Fire in October 2017, the Thomas Fire in December 2017, the Mendocino and Carr fires in summer 2018 (9), and the Woolsey and tragic Camp fires in November 2018 (6).

Most climate simulations agree that CA will warm in the 21st century (10), but the projections for future precipitation patterns—strongly linked to North Pacific jet stream (NPJ) dynamics that regulate moisture delivery from the Pacific Ocean—are less unanimous. During the 2012 to 2015 drought in CA, the North Pacific blocking ridge was unusually persistent ("the ridiculously resilient ridge") and formed a dipole with an equally persistent trough over east-central to far northeastern North America (11) (*SI Appendix*, Fig. S1); this dipole pattern has been linked to a warming North Pacific Ocean (12). The association between North Pacific blocking and CA drought is also reflected in increased CA fire risk (13) and annual area burned (14) and is consistent with paleoclimate reconstructions of high sea-level pressure for extreme dry years in CA (15). During the winter of 2015/2016, the blocking ridge was significantly reduced in strength, and its center in western North America had shifted northeastward into Canada (*SI Appendix*, Fig. S1). By the winter of 2016/2017, a deep low pressure anomaly covered much of the mid- to high-latitude North Pacific (*SI Appendix*, Fig. S1), allowing NPJ-driven Pacific storm tracks to deliver large amounts of moisture into CA, notably in the form of atmospheric rivers (16).

Significance

North Pacific jet stream (NPJ) behavior strongly affects cool-season moisture delivery in California and is an important predictor of summer fire conditions. Reconstructions of the NPJ before modern fire suppression began in the early 20th century identify the relationships between NPJ characteristics and precipitation and fire extremes. After fire suppression, the relationship between the NPJ and precipitation extremes is unchanged, but the NPJ–fire extremes relationship breaks down. Simulations with high CO_2 forcing show higher temperatures, reduced snowpack, and drier summers by 2100 whether overall precipitation is enhanced or reduced, thereby overriding historical dynamic NPJ precursor conditions and increasing fire potential due to thermodynamic warming. Recent California fires during wet extremes may be early evidence of this change.

With drought and large precipitation events (8) and CA fire weather projected to become more extreme with anthropogenic climate changes (17), it is essential to improve our understanding of North Pacific circulation as a driver of extreme events to anticipate future socioenvironmental impacts. Here, we present a 400-y reconstruction of NPJ variability to understand its impact on historical CA precipitation and wildfire over much of the past half-millennium. For this analysis, we use an off-line paleo data assimilation scheme (18) to reconstruct atmospheric circulation at 200 hPa geopotential height (an atmospheric level typically used to characterize the behavior of the NPJ) during Northern Hemisphere winter (December$_{t-1}$ to February$_t$), the months CA receives more than half its annual precipitation (19). The reconstruction spans the period 1571 to 1977 and focuses on developing reconstruction skill for the sectors most relevant for CA precipitation: the northeastern Pacific Ocean and coastal western North America. The primary Earth System Model (ESM) we employ is the Max Planck Institute (MPI)-ESM-P (see *Methods* and *SI Appendix* for

details of the reconstruction and criteria for ESM selection). Our reconstruction represents an important extension for this region in last-millennium paleoclimatology, which seeks to develop spatially explicit, annually resolved reconstructions of precipitation and circulation fields (cf. refs. 18 and 20–22).

We couple the NPJ reconstruction with a separate paleo-reconstruction of Sierra Nevada precipitation (23) and an index of Sierra Nevada fire extent (24) to identify NPJ influence on extreme dry/wet and high/low fire years in CA. The fire index measures fire activity as recorded in tree rings (1600 to 1907) and historical fire records (1908 to 2015) across the entire length of the Sierra Nevada, and represents fire extent at a regional scale appropriate for comparison with synoptic-scale NPJ reconstructions (see *Methods* and *SI Appendix*, Fig. S2). Four fire regimes linked to distinct socioecological conditions are evident in the fire record (24), and we stratify our results and analyses across them. The regimes include precontact Native American subsistence burning (1600 to 1775), postcontact disruption and native American
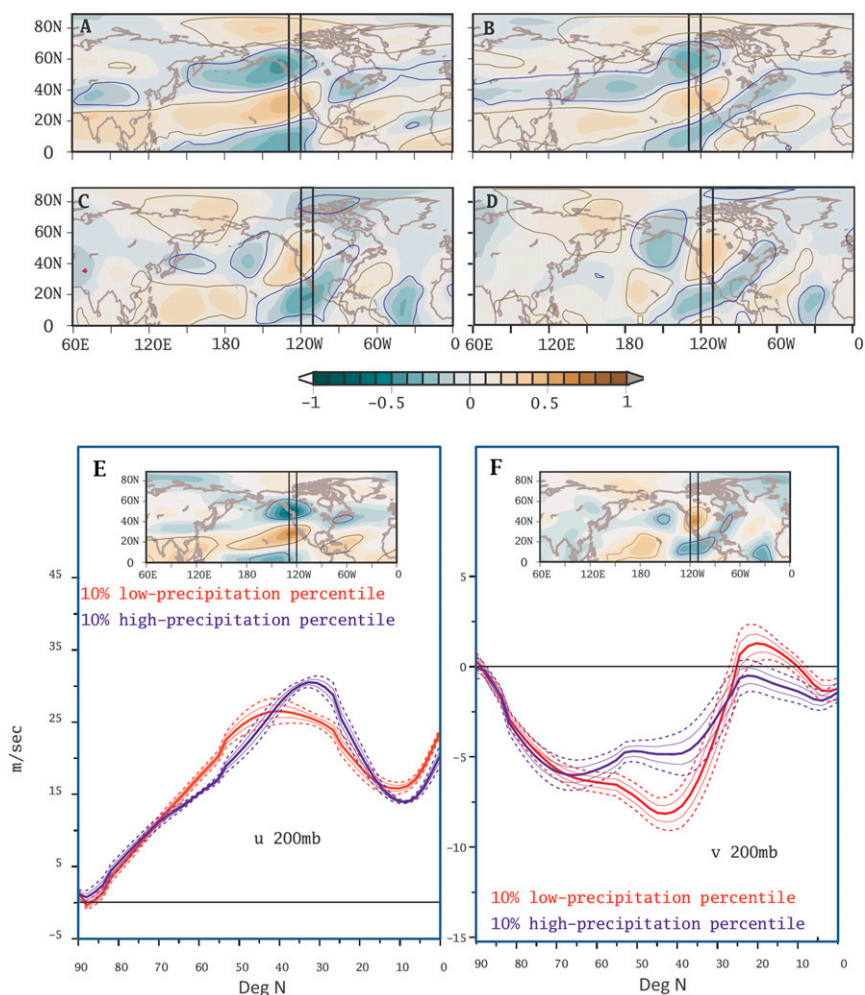

Fig. 1. Linkages between winter NPJ winds and CA precipitation or fire activity. (*A–D*) Correlation maps between reconstructed Sierra Nevada precipitation (23) or fire activity (24) and zonal (*u*) and meridional (*v*) components of the winter (December$_{t-1}$ to February$_t$) 200 hPa wind reconstructed from the MPI-ESM-P model: precipitation and NPJ$_u$ (*A*), fire activity (inverted) and NPJ$_u$ (*B*), precipitation and NPJ$_v$ (*C*), and fire activity (inverted) and NPJ$_v$ (*D*). Rectangles show longitudinal windows where correlations between the wind components and precipitation or fire activity are jointly highest (120° to 130°W for NPJ$_u$; 110° to 120°W for NPJ$_v$), and used for analysis of maximum winds. Time periods are 1571 to 1903 for precipitation (to earliest year of NPJ data) and 1600 to 1903 for fire activity (to earliest year of fire data). (*E–F*) Latitudinal profiles of 200 hPa NPJ$_u$ wind velocity averaged between 120°W and 130°W (*E*) and 200 hPa NPJ$_v$ wind velocity averaged between 110°W and 120°W (*F*), for the 10% driest (red) and 10% wettest (blue) winters in CA during the period 1904 to 2013, according to the 20CR (26). Thick solid lines indicate mean values at each latitude for each set of winters; thin solid lines and dashed lines indicate ±1 and ±2 sample-estimated SEM, respectively. *Insets* show correlations maps for 20CR precipitation and NPJ$_u$ (*E*) or NPJ$_v$ (*F*), as in *A* or *C*, respectively. Contour lines in correlation plots (*A–F*) indicate $P < 0.05$ significance levels (brown, positive; blue, negative), corrected for autocorrelation for each grid-cell time series (52).

Wahl et al.

depopulation (1776 to 1865), intensification of Euro-American forest use in the late 19th century (1866 to 1903), and the period of modern fire suppression (1904 to present) (24). An additional regime subdivision was added at 1977 to isolate the later part of the 20th and early 21st centuries when there were state changes in the northern Pacific Ocean (25), temperature, and increased fire extent (17, 19, 24); during this period, the 20th Century Reanalysis v2 (20CR) (26) is employed in combination with the fire record for analysis. The combination of high-resolution paleoclimate and paleofire activity allows characterization of the mechanistic relationship among NPJ behavior, moisture delivery, and fire extent over a period nearly four times longer than the instrumental record, including a spectrum of human-modulated fire regimes.

We first characterize the relationship between CA precipitation and 200 hPa wind in the 20CR and compare it to the corresponding reconstruction results, utilizing the independence of the reanalysis to validate the reconstruction information. The spatial pattern of correlation between CA winter precipitation and the winter 200 hPa wind field for the reanalysis (1904 to 2013; Fig. 1 E and F, *Insets*) is very similar to the spatial correlation between CA precipitation or fire activity and the winter 200 hPa wind field for the reconstruction (Fig. 1 A–D). Low precipitation extremes in the reanalysis (Fig. 1E, red curve) and reconstructed pre–20th-century extremes for both dry and high-fire conditions (defined as $\leq 10\%$ and $\geq 90\%$ of their distributions, respectively) (Fig. 2 A and C, red curves) are strongly associated with a weakening, a northward-shifted extent, and a wider latitudinal spread of maximum velocity, centered at $\sim$39 to 41° N, for the NPJ zonal (u) component (NPJ_u) in the northeastern Pacific and far western North America. Conversely, extreme wet and low-fire conditions (defined as $\geq 90\%$ and $\leq 10\%$ of their distributions, respectively) are strongly associated with a strengthening, a southward-shifted extent, and a narrower latitudinal spread of NPJ_u maximum velocity, centered at $\sim$33 to 34° N (Figs. 1E and 2 A and C, blue curves), which increases precipitation from northern Pacific storm track activity and moist tropical airflow into CA. The NPJ meridional (v) component (NPJ_v) is stronger and more negative in the study region during dry extremes (Figs. 1F and 2B, red curves), corresponding to more northerly flow and a characteristic blocking high-pressure ridge (*SI Appendix*, Fig. S1); the same NPJ_v pattern is evident for high-fire years (Fig. 2D, red curve). The generally close correspondence of the reanalysis and reconstruction precipitation results over the common 1904 to 1977 period (Figs. 3 A and B and 4 D and H) serves as additional validation of the NPJ reconstruction (*SI Appendix, Additional Methodological Detail* and Figs. S5D and S6D), along with the Sierra Nevada precipitation and fire data used to evaluate moisture and fire extremes relationships for the paleoreconstruction period evaluated here.

The relationship of the NPJ to precipitation and fire extremes (Figs. 4 and 5) remains largely constant in the reconstructions throughout 1600 to 1977, despite the four distinct regimes of fire extent related to changes in human activity. Separation of the precipitation and fire extremes in terms of NPJ_u maximum velocity is relatively weaker during the 1904 to 1977 period with fire suppression compared with earlier fire regimes (Figs. 4D and 5D), and is most evident for the extreme dry case (Fig. 4D, red curve). The maximum of NPJ_v exhibits a southward shift coupled with a relatively steeper latitudinal gradient over CA for the extreme wet case during the 1600 to 1775 and the 1904 to 1977 regimes (Fig. 4 E and H, blue curves). This feature indicates that the wet and low-fire extreme years were more distinct during these two regimes than during the two intervening ones (1776 to 1903) and that the difference was primarily evident in NPJ_v.

The effect of modern fire suppression management on the NPJ–fire extremes relationship is even more evident in the reanalysis data (Fig. 3 E–H), covering 1904 to 2013. As with the reconstruction, there is statistically meaningful separation in NPJ_u maximum velocity between high- and low-fire extremes
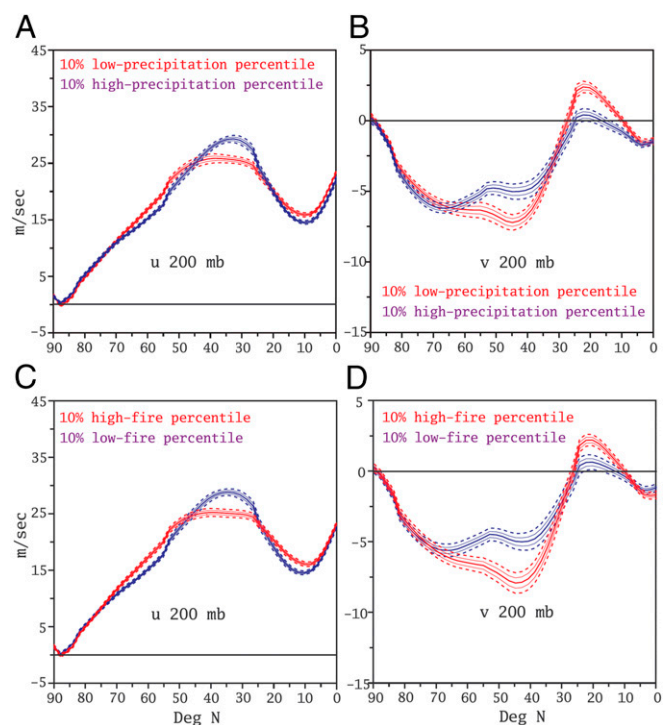

Fig. 2. Latitudinal profiles of reconstructed winter NPJ wind velocity for extreme precipitation and fire years in CA, before modern fire suppression. (*A*) Mean 200 hPa NPJ_u wind velocity for the 10% driest (red) and 10% wettest (blue) winters according to reconstructed Sierra Nevada precipitation (23). (*B*) As for *A*, but for the mean 200 hPa NPJ_v wind. (*C*) Mean 200 hPa NPJ_u wind for years with the 10% highest (red) and 10% lowest (blue) Sierra Nevada fire activity (24). (*D*) As for *C*, but for the mean 200 hPa NPJ_v wind. Thick solid lines indicate mean values at each latitude for each set of winters; thin solid lines and dashed lines indicate ±1 and ±2 sample-estimated SEM, respectively. Jet stream winds are averaged between 120°W and 130°W for the NPJ_u, and between 110°W and 120°W for the NPJ_v. Time periods are 1571 to 1903 for precipitation extremes (to earliest year of NPJ data) and 1600 to 1903 for fire extremes (to earliest year of fire data).

during the 1904 to 1977 period (Figs. 3E and 5D), but there is much less separation than for the corresponding extreme precipitation cases (Fig. 3A). More notably, NPJ_u maximum velocity for the extreme low-fire case is reduced and shifted to northern CA at $\sim$40° N, and the flatness of the velocity profile for the high-fire case extends to northern Mexico (Fig. 3E). During the 1978 to 2013 period, there is no difference in NPJ_u between the high- and low-fire cases (Fig. 3G), in clear contrast to the differences for NPJ_u for the extreme precipitation cases (Fig. 3C), notwithstanding widening of estimated uncertainty ranges for this period relative to the 1904 to 1977 period (compare with Fig. 3A) due to the shorter time span covered. Similarly, there is no difference in NPJ_v between the high- and low-fire cases throughout the post-1904 period (Fig. 3 F and H), again in clear contrast to the 1904 to 1977 extreme precipitation cases (Fig. 3B), but with less contrast to the 1978 to 2013 precipitation extremes (Fig. 3D). The steepness and amplitude of the latitudinal gradient of NPJ_v in the CA region continues to be greater for the high-fire versus low-fire cases during this time (Fig. 3 F and H). Notably, however, both cases exhibit greater range in NPJ_v amplitude, and the gradient steepness for the low-fire case is stronger than in the corresponding reconstruction results (Fig. 5H) and the reanalysis extreme precipitation case during 1904 to 1977 (Fig. 3B). The erosion of 20th-century NPJ–fire relationships and the full uncoupling of fire from NPJ_u after 1977 document the recent amplification of fire regime regulation by humans.
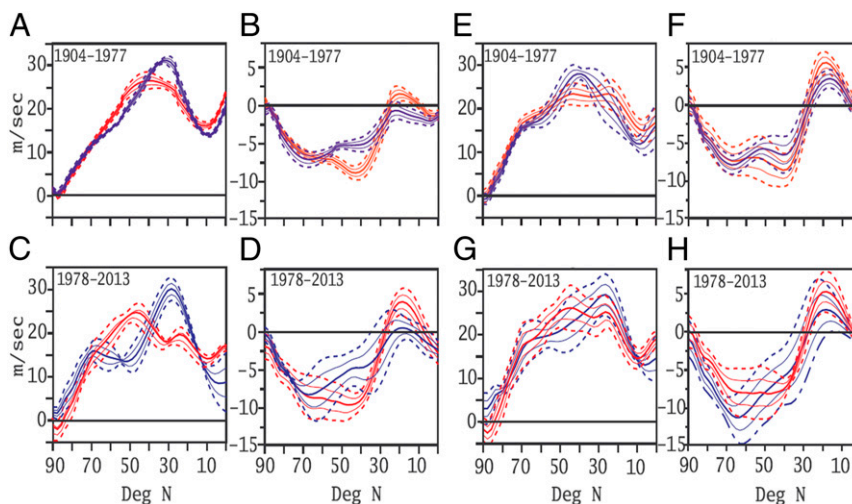
Fig. 3. NPJ$_u$ and NPJ$_v$ wind behavior related to precipitation (*A–D*) and fire (*E–H*) extremes over social usage regime subdivisions, 1904 to 2013. (*A* and *C*) As for Fig. 1*E* for 200 hPa NPJ$_u$ wind associated with precipitation extremes from the 20CR (26), including the fire regime subdivision at 1977 described in the text. (*B* and *D*) As for Fig. 1*F* for 200 hPa NPJ$_v$ wind associated with precipitation extremes from the 20CR, including fire regime subdivision at 1977. (*E* and *G*) As for *A* and *C*, but for 200 hPa NPJ$_u$ wind from the 20CR associated with fire extremes (24). (*F* and *H*) As for *B* and *D*, but for 200 hPa NPJ$_v$ wind from the 20CR associated with fire extremes.

Our results complement and extend two recent studies that focus on wet-season cyclonic storm track position (strongly associated with the NPJ) in the Pacific Northwest region of the United States. The first (27) presents index reconstructions of storm track latitudes across a set of longitudinal transects for the period 1693 to 1995; the second (28) evaluates the recent period of 1980 to 2014 and relates storm track position to forest growth and fire activity in western North America. The Pacific Northwest is the region of typical wet-season storm entry into mid-latitude western North America (28, 29), and relatively subtle differences in the central storm track latitude there can have a large influence on regional hydroclimate (27). In contrast, much of CA lies south of the general northeastern Pacific storm track, and relatively large, transient latitudinal excursions of the storm track center are strongly associated with winter moisture delivery

(29), as noted here (Figs. 1*E*, 2*A*, 3 *A* and *C*, and 4 *A–D*). Our reconstructions extend examination of storm track-related NPJ behavior along the Pacific Coast over a century further into the past and, importantly, provide a full, physically consistent reconstruction of the 200 hPa atmospheric circulation for a large portion of the northeastern Pacific region and adjacent North America to 1571 (see *Data Availability*). Additionally, we couple this longer circulation record with corresponding precipitation and fire activity records in the Sierra Nevada, including socially driven changes in fire activity, providing an opportunity to evaluate the combined relationships of paleocirculation, paleoprecipitation, and paleofire to inform understanding of drivers of precipitation and fire in CA forests since 1600.

Climate models generally agree that temperatures are projected to increase in the future (10), and this, in association with
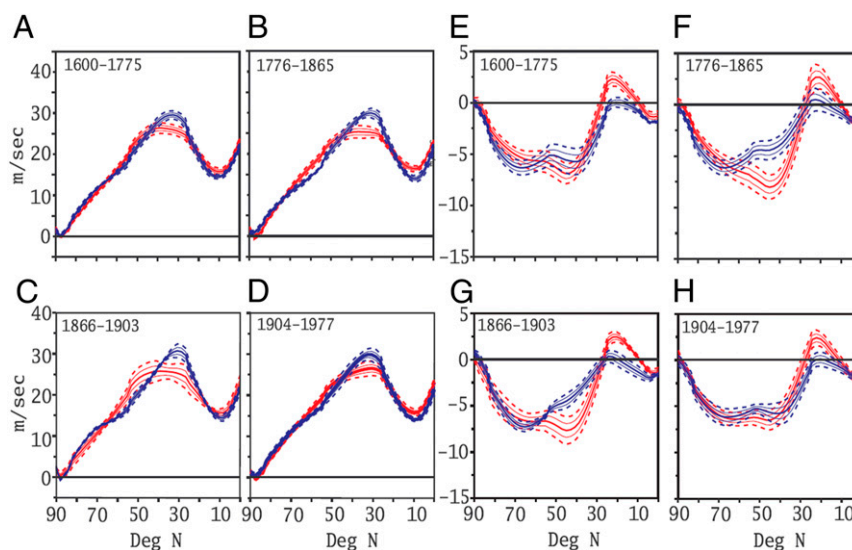

Fig. 4. NPJ$_u$ and NPJ$_v$ wind behavior related to precipitation extremes over social usage regimes, 1600 to 1977. (*A–D*) As for Fig. 2*A* for 200 hPa NPJ$_u$ wind associated with precipitation extremes from reconstruction, for fire regime periods defined in ref. 24. (*E–H*) As for Fig. 2*B* for 200 hPa NPJ$_v$ wind associated with precipitation extremes from reconstruction, for fire regime periods.
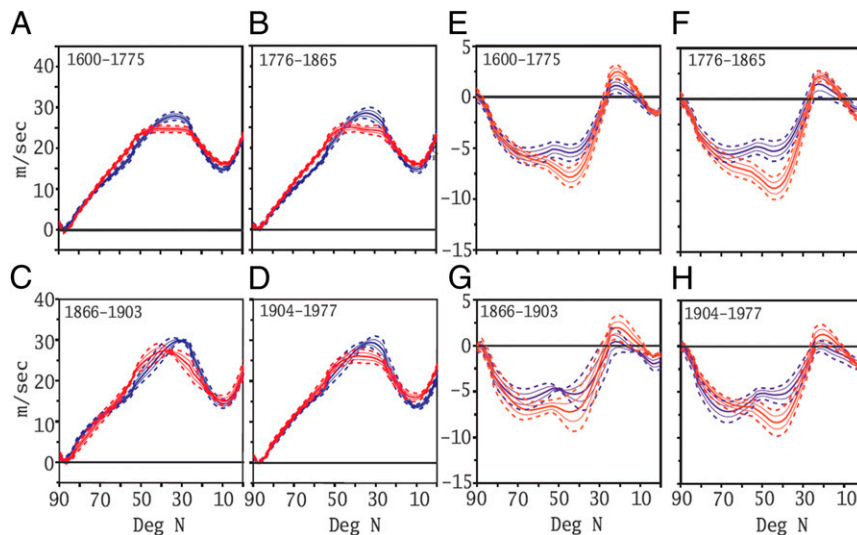
Fig. 5. NPJ$_u$ and NPJ$_v$ wind behavior related to fire extremes over social usage regimes, 1600 to 1977. (*A–D*) As for Fig. 2*C* for 200 hPa NPJ$_u$ wind associated with fire extremes from reconstruction, for fire regime periods defined in ref. 24. (*E–H*) As for Fig. 2*D* for 200 hPa NPJ$_v$ wind associated with fire extremes from reconstruction, for fire regime periods.

enhanced vapor pressure deficits that are already occurring (30), will increase warm-season fire risk (17). The models have less convergence regarding antecedent cool-season precipitation (31). While most of the Coupled Model Intercomparison Project Phase 5 models project at least a small increase in winter precipitation over most of CA under the representative concentration pathway (RCP)8.5 scenario, a minority do not (31); this reduced convergence is likely due to the location of CA in the transition zone between simulated midlatitude increases and subtropical decreases in precipitation (31) and to regional heterogeneity in the projected future shift of the midlatitude jets (32). The MPI-ESM-P model we utilize for paleo- and modern-period analysis is in the model majority and simulates winter NPJ conditions under the RCP8.5 scenario that are most consistent with the pre–20th-century high-precipitation/low-fire state (*SI Appendix*, Fig. S3). In conjunction with increasing temperatures, however, more of this winter precipitation would occur as rain relative to snow (33) (*SI Appendix*, Fig. S4*D*), reducing snowpack duration (34) and, along with enhanced vapor pressure deficits (30), would lead to earlier warm-season forest drying compared with the same NPJ conditions before modern fire suppression. Thus, by the later 21st century, the relationship of fire extremes and winter climate precursor conditions in CA montane forests could potentially have no ecological parallel compared with winter conditions before modern fire suppression. In terms of climate physics, while winter precursor conditions for CA wildfire were strongly dynamically driven by NPJ activity before modern fire suppression (Figs. 2 *C* and *D* and 5 *A–C* and *E–G*), potential future increases in temperature and corresponding reductions in the snow-to-rain ratio would result in a shift to fire conditions (separate from suppression efforts per se) that are more thermodynamically controlled, both in terms of the winter precursor conditions and summer "fire weather" itself (35). The recent widespread fires in CA's forests (6, 9) may be early evidence of this change; in our record, the presuppression period of 1600 to 1903 does not contain a single case of a high-precipitation year coupled with a high-fire year, as occurred in 2017.

If it occurs, such a fundamental reorganization of climate controls will not only likely promote the incidence of "megafires" (36) in fuel-rich forests that have experienced a century of fire suppression (37), but also entrain second- and third-order effects that alter species distributions, forest composition, and ecosystem function (i.e., productivity and carbon and water cycling) (38). Our work provides a critical multicentury perspective on the physical drivers of climate that could reorganize CA forest ecosystems and their disturbances. It also provides a stronger foundation and a longer-term perspective for evaluating regional natural hazards and economic risk to CA under the RCP8.5 scenario in one of the world's largest economies.

Methods

Atmospheric Circulation Field Reconstruction. We used an analog assimilation method similar to that applied in other studies (18, 39–42) to reconstruct 3D fields of the atmospheric circulation, based on a combination of state-of-the-art climate model output [MPI-ESM-P (43), National Center for Atmospheric Research Community Climate System Model, version 4 (44), and Goddard Institute for Space Studies Model E2-R (45) last-millennium transient-forcing simulations; see *SI Appendix, Earth System Model Selection and Evaluation*] and three gridded paleoclimate reconstructions. The reconstruction predictors include tree ring-based reconstructions of June to August$_t$ soil moisture [the North American Drought Atlas (NADA)] (46), water-year$_t$ (October$_{t-1}$ through September$_t$) precipitation (15, 20), and February to March$_t$ near-surface air temperature (47) over portions of western and southwestern North America. For a given calendar year *t*, the predictor fields are compared with the simulated seasonal mean fields of the same variables through the length of the climate simulations; the years for which the simulated seasonal fields are most similar to the gridded reconstructions are considered the "analog years," and the atmospheric circulation (the predictand) of the corresponding winter (December$_{t-1}$ to February$_t$) season is selected to form the model-based reconstruction. To define the most similar analogs, the three climate variables were merged into a single vector for each year after they were regridded to a common 2.5 × 2.5 longitude/latitude grid and then normalized so that each variable had the same weight in the definition of similarity to the simulation output.

The physical basis for this strategy is the strong relationship between these variables and the winter atmospheric circulation over the northeastern Pacific–western North American sector. Winter temperatures are directly influenced by this circulation via air mass advection, and the two hydrological variables also strongly depend on the moisture delivery from the Pacific onto land that occurs during the winter season. As noted, CA receives more than half its annual precipitation during winter (19), and the NADA has been shown to be strongly related to antecedent winter moisture delivery south and west of a line connecting the northwestern United States to northeastern Mexico (48), which is the regional portion utilized here. Employing the analog method, the global 3D field of the atmospheric circulation can, in principle, be reconstructed, although the actual reconstruction skill will be spatially heterogeneous and generally focused in the regions where the atmospheric circulation most strongly influences the predictors (*SI Appendix*, Figs. S5 and S6). We note the similarity of this reconstruction process to the Proxy Surrogate Reconstruction method outlined in ref. 49.

We extracted 200 hPa zonal (u) and meridional (v) wind components from the reconstructed circulation fields for analysis of winter NPJ conditions. We analyzed the latitudinal position and strength of the reconstructed NPJ during extreme wet/dry years in CA using a tree ring-based reconstruction of October$_{t-1}$ to June$_t$ precipitation for the southern Sierra Nevada mountains (23), which is nearly independent of the NPJ reconstruction. In a similar way, we stratified NPJ winter conditions according to high- and low-fire years, as reconstructed from a completely independent record of Sierra Nevada fire history (24) (SI Appendix, Fig. S2). We note that the annual precipitation at the fire record sites is generally similar to that in the precipitation reconstruction subregion, which is included within the spatial extent of the fire record near its southern end (50). We also note that the spatial coverage of the extreme precipitation stratification in the 20CR (Figs. 1 E and F and 3 A–D) is spatially as close to the independent Sierra Nevada paleoprecipitation record as possible, given the gridded nature of the reanalysis, and that the 20CR seasonal coverage also matches that of the Sierra Nevada record (October$_{t-1}$ to June$_t$).

As noted, winter dates are labeled according to the year in which January occurs. Winter 2013 values from the 20CR are based on December 2012, the end of the 20CR record. Further methodological information is provided in the SI Appendix, Additional Methodological Detail.

Data Availability. The 200 hPa geopotential height and corresponding NPJ$_u$ and NPJ$_v$ wind reconstructions are housed with the World Data Service for Paleoclimatology, https://www.ncdc.noaa.gov/paleo-search/ (51).

1. Bartos MD, Chester MV (2015) Impacts of climate change on electric power supply in the western United States. *Nat Clim Chang* 5:748–752.
2. Asner GP, et al. (2016) Progressive forest canopy water loss during the 2012-2015 California drought. *Proc Natl Acad Sci USA* 113:E249–E255.
3. Brown EG, Jr (2017) Governor of California lifts drought restrictions. Available at https://www.gov.ca.gov/wp-content/uploads/2017/09/4.7.17_Exec_Order_B-40-17.pdf. Accessed February 7, 2019.
4. Belmecheri S, Babst F, Wahl ER, Stahle DW, Trouet V (2016) Multi-century evaluation of Sierra Nevada snowpack. *Nat Clim Chang* 6:2–3.
5. Serna J (August 10, 2017) California received $22 million from FEMA for Oroville Dam emergency. *Los Angeles Times*. Available at www.latimes.com/local/lanow/la-me-ln-oroville-fema-payment-20170810-story.html. Accessed February 7, 2019.
6. CALFIRE (2018) Incident information. Available at cdfdata.fire.ca.gov/incidents/incidents_statsevents. Accessed October 1, 2018 and February 12, 2018.
7. Diffenbaugh NS, Swain DL, Touma D (2015) Anthropogenic warming has increased drought risk in California. *Proc Natl Acad Sci USA* 112:3931–3936.
8. Dettinger M (2011) Climate change, atmospheric rivers, and floods in California–A multimodel analysis of storm frequency and magnitude changes. *J Am Water Resour Assoc* 47:514–523.
9. Abatzoglou JT, Balch JK, Bradley BA, Kolden CA (2018) Human-related ignitions concurrent with high winds promote large wildfires across the USA. *Int J Wildland Fire* 27:377–386.
10. Pierce DW, et al. (2013) Probabilistic estimates of future changes in California temperature and precipitation using statistical and dynamical downscaling. *Clim Dyn* 40:839–856.
11. Swain DL, et al. (2014) The extraordinary California drought of 2013/2014: Character, context, and the role of climate change. *Bull Am Meteorol Soc* 95:S3–S7.
12. Funk C, Hoell A, Stone D (2014) Examining the contribution of the observed global warming trend to the California droughts of 2012/13 and 2013/14. *Bull Am Meteorol Soc* 95:S11–S15.
13. Trouet V, Taylor AH, Carleton AM, Skinner CN (2009) Interannual variations in fire weather, fire extent, and synoptic-scale circulation patterns in northern California and Oregon. *Theor Appl Climatol* 95:349–360.
14. Trouet V, Taylor AH, Carleton AM, Skinner CN (2006) Fire-climate interactions in forests of the American Pacific coast. *Geophys Res Lett* 33:L18704.
15. Diaz HF, Wahl ER (2015) Recent California water year precipitation deficits: A 440-year perspective. *J Clim* 28:4637–4652.
16. Neiman PJ, Ralph FM, Wick GA, Lundquist JD, Dettinger MD (2008) Meteorological characteristics and overland precipitation impacts of atmospheric rivers affecting the West Coast of North America based on eight years of SSM/I satellite observations. *J Hydrometeorol* 9:22–47.
17. Westerling AL (2016) Increasing western US forest wildfire activity: Sensitivity to changes in the timing of spring. *Philos Trans R Soc Lond B Biol Sci* 371:20150178.
18. Diaz HF, Wahl ER, Zorita E, Giambelluca TW, Eischeid JK (2016) A five-century reconstruction of Hawaiian Islands winter rainfall. *J Clim* 29:5661–5674.
19. NOAA National Centers for Environmental Information (2019) Climate at a glance: Statewide time series. Available at https://www.ncdc.noaa.gov/cag/statewide/time-series. Accessed February 7, 2019.
20. Wahl E, Diaz H, Vose R, Gross W (2017) Multi-century evaluation of recovery from strong precipitation deficits in California. *J Clim* 30:6053–6063.
21. Wise EK (2016) Five centuries of U.S. West Coast drought: Occurrence, spatial distribution, and associated atmospheric circulation patterns. *Geophys Res Lett* 43:4539–4546.
22. Wise EK, Dannenberg MP (2014) Persistence of pressure patterns over North America and the North Pacific since AD 1500. *Nat Commun* 5:4912.
23. Graumlich LJ (1993) A 1000-year record of temperature and precipitation in the Sierra Nevada. *Quat Res* 39:249–255.
24. Taylor AH, Trouet V, Skinner CN, Stephens S (2016) Socioecological transitions trigger fire regime shifts and modulate fire-climate interactions in the Sierra Nevada, USA, 1600-2015 CE. *Proc Natl Acad Sci USA* 113:13684–13689.
25. Hare S, Mantua N (2000) Empirical evidence for North Pacific regime shifts in 1977 and 1989. *Prog Oceanogr* 47:103–145.
26. Compo GP, et al. (2011) The twentieth century reanalysis project. *Q J R Meteorol Soc* 137:1–28.
27. Wise EK, Dannenberg MP (2017) Reconstructed storm tracks reveal three centuries of changing moisture delivery to North America. *Sci Adv* 3:e1602263.
28. Dannenberg MP, Wise EK (2017) Shifting Pacific storm tracks as stressors to ecosystems of western North America. *Glob Change Biol* 23:4896–4906.
29. Swain DL, Horton DE, Singh D, Diffenbaugh NS (2016) Trends in atmospheric patterns conducive to seasonal precipitation and temperature extremes in California. *Sci Adv* 2:e1501344.
30. Abatzoglou JT, Williams AP (2016) Impact of anthropogenic climate change on wildfire across western US forests. *Proc Natl Acad Sci USA* 113:11770–11775.
31. Chang EKM, Zheng C, Lanigan P, Yau AMW, Neelin JD (2015) Significant modulation of variability and projected change in California winter precipitation by extratropical cyclone activity. *Geophys Res Lett* 42:5983–5991.
32. Simpson IR, Seager R, Ting MF, Shaw TA (2016) Causes of change in Northern Hemisphere winter meridional winds and regional hydroclimate. *Nat Clim Chang* 6:65–70.
33. Ashfaq M, et al. (2013) Near-term acceleration of hydroclimatic change in the western US. *J Geophys Res Atmos* 118:10676–10693.
34. Huang X, Hall AD, Berg N (2018) Anthropogenic warming impacts on today's Sierra Nevada snowpack and flood risk. *Geophys Res Lett* 45:6215–6222.
35. Trouet V, Taylor AH, Wahl ER, Skinner CN, Stephens SL (2010) Fire-climate interactions in the American West since 1400 CE. *Geophys Res Lett* 37:L04702.
36. Adams MA (2013) Mega-fires, tipping points and ecosystem services: Managing forests and woodlands in an uncertain future. *For Ecol Manage* 294:250–261.
37. Dennison PE, Brewer SC, Arnold JD, Moritz MA (2014) Large wildfire trends in the western United States, 1984-2011. *Geophys Res Lett* 41:2928–2933.
38. Liang S, Hurteau MD, Westerling AL (2017) Potential decline in carbon carrying capacity under projected climate-wildfire interactions in the Sierra Nevada. *Sci Rep* 7:2420.
39. Schenk F, Zorita E (2012) Reconstruction of high resolution atmospheric fields for Northern Europe using analog-upscaling. *Clim Past* 8:1681–1703.
40. Ohlwein C, Wahl ER (2012) Review of probabilistic pollen-climate transfer methods. *Quat Sci Rev* 31:17–29.
41. Wahl ER (2004) A general framework for determining cutoff values to select pollen analogs with dissimilarity metrics in the modern analog technique. *Rev Palaeobot Palynol* 128:263–280.
42. Gavin DG, Oswald WW, Wahl ER, Williams JW (2003) A statistical approach to evaluating distance metrics and analog assignments for pollen records. *Quat Res* 60:356–367.
43. Giorgetta MA, et al. (2013) Climate and carbon cycle changes from 1850 to 2100 in MPI-ESM simulations for the coupled model intercomparison project phase 5. *J Adv Model Earth Syst* 5:572–597.
44. Landrum L, et al. (2013) Last millennium climate and its variability in CCSM4. *J Clim* 26:1085–1111.
45. Schmidt GA, et al. (2014) Configuration and assessment of the GISS ModelE2 contributions to the CMIP5 archive. *J Adv Model Earth Syst* 6:141–184.
46. Cook ER, et al. (2010) Megadroughts in North America: Placing IPCC projections of hydroclimatic change in a long-term palaeoclimate context. *J Quat Sci* 25:48–61.
47. Wahl ER, Diaz HF, Smerdon JE, Ammann CM (2014) Late winter temperature response to large tropical volcanic eruptions in temperate western North America: Relationship to ENSO phases. *Global Planet Change* 122:238–250.
48. St George S, Meko DM, Cook ER (2010) The seasonality of precipitation signals embedded within the North American Drought Atlas. *Holocene* 20:983–988.
49. Graham NE, et al. (2007) Tropical Pacific—Mid-latitude teleconnections in medieval times. *Clim Change* 83:241–285.
50. Western Regional Climate Center. (1995) Average annual precipitation (inches), California. Period: 1961-1991. Available at https://wrcc.dri.edu/Climate/precip_map_show.php?simg=ca.gif. Accessed July 26, 2018.
51. Wahl ER, et al. (2018) "Data for the 200 hPa geopotential height and corresponding NPJ u- and v-wind reconstructions." NOAA World Data Service for Paleoclimatology. Available at https://www.ncdc.noaa.gov/paleo/study/26030. Deposited February 8, 2019.
52. Ebisuzaki W (1997) A method to estimate the statistical significance of a correlation when the data are serially correlated. *J Clim* 10:2147–2153.